Characterization of xylitol or citric acid:choline chloride:water mixtures: Structure, thermophysical properties, and quercetin solubility

Noelia López[a], Ignacio Delso[b], David Matute[a], Carlos Lafuente[a], and Manuela Artal[a,*]

[a]Departamento de Química Física, Universidad de Zaragoza, Zaragoza, Spain

[b]Departamento de Síntesis y Estructura de Biomoléculas, Instituto de Síntesis Química y Catálisis Homogénea (ISQCH), Universidad de Zaragoza-CSIC, Spain

*Corresponding author. Tel: +34876553765. e-mail: martal@unizar.es

ABSTRACT

The industrial implementation of new eco-friendly solvents has highlighted the need to analyse both the structures and thermophysical properties of these solvents. Here, two deep eutectic solvents (DESs) used in the agro-food field were studied: xylitol:choline chloride:water (1:2:3 molar ratio), XoCH, and citric acid:choline chloride:water (1:1:6 molar ratio), CiCH. The H-bond network between the components of each DES was evaluated and the diffusion coefficients at 298.15 K were calculated using NMR spectroscopy. In addition, seven thermophysical properties were determined from 278.15 to 338.15 K. Also, the solubility of quercetin in water and in the two eutectic mixtures was measured and the interactions between components were studied. NMR experiments revealed the presence of water within the supramolecular structure of XoCH, but CiCH is a "DES-in-water" solution. Based on the results, XoCH is the most compact mixture. Finally, quercetin was remarkably more soluble in the studied DESs than in pure water.

Keywords: DES, Quercetin, Choline chloride, NMR, Thermophysical properties, Solubility

1. Introduction

An adequate design for an industrial process requires knowledge of the physicochemical behaviours of the solvents involved in the process. Using green chemistry principles, new solvents with a low environmental impact must be developed. Among other solvents (supercritical fluids, liquid polymers, and biomass-derived liquids), deep eutectic solvents (DESs) are currently highlighted (Clarke, Tu, Levers, Bröhl, & Hallett, 2018; Pena-Pereira, Kloskowski, & Namieśnik, 2015). DESs are mixtures of compounds that are able to establish a hydrogen bond network with a fusion temperature less than the ideal mixture (Martins, Pinho, & Coutinho, 2018). The interactions between the donor and acceptor components are the origin of the supramolecular structure detected in NMR studies (Posada et al., 2017). Many compounds with diverse chemical properties can function as hydrogen acceptors and hydrogen donors, and thus the number of possible eutectics is very high. Notably, the composition of the studied DESs is frequently different from the eutectic point of the mixture reported in the literature. The utility of DESs has been confirmed in different applications: solvents, additives and monomers in polymerization; extraction, detection, and electrodeposition of metals; extraction of bioactive compounds; reaction medium in the synthesis of organic compounds and nanomaterials; and several biomedical uses (Clarke et al., 2018; Dai, Witkamp, Verpoorte, & Choi, 2015; Deng et al., 2019; Espino, de los Ángeles Fernández, Gomez, & Silva, 2016; García, Rodríguez-Juan, Rodríguez-Gutiérrez, Rios, & Fernández-Bolaños, 2016; Huang, Feng, Chen, Wu, & Wang, 2018; Zainal-Abidin, Hayyan, Hayyan, & Jayakumar, 2017).

The high viscosity of many DESs is an important limitation preventing their implementation in industry. However, the addition of small quantities of water causes a considerable increase in the fluidity. Therefore, an interesting issue is the effect of water

both on the structure and the properties of DESs (Dai et al., 2015; Delso, Lafuente, Muñoz-Embid, & Artal, 2019; Hammond, Bowron, & Edler, 2017; Lapeña, Lomba, Artal, Lafuente, & Giner, 2019; Zhekenov, Toksanbayev, Kazakbayeva, Shah, & Mjalli, 2017). In the present study, we characterize two aqueous eutectic solvents whose composition is xylitol:choline chloride:water (1:2:3) and citric acid:choline chloride:water (1:1:6). The abbreviations used in this article will be XoCH and CiCH, respectively. The water content was chosen to obtain an adequate fluidity of both solvents. These DESs have been already used in the field of biotechnology both in the extraction of flavonoids, anthocyanins, and phenolic compounds, and in the solubilisation of proteins and substances with poor water solubility (Bajkacz & Adamek, 2018; Bosiljkov et al., 2017; Dai, van Spronsen, Witkamp, Verpoorte, & Choi, 2013; García et al., 2016; Lores, Romero, Costas, Bendicho, & Lavilla, 2017; Tang, Zhong, & Yan, 2016). Several papers describing some properties of these mixtures have been published (Abbott, Boothby, Capper, Davies, & Rasheed, 2004; Altamash et al., 2017; Aroso, Paiva, Reis, & Duarte, 2017; Craveiro et al., 2016; Crespo et al., 2018; Dai et al., 2013; Maugeri & Domínguez De María, 2012; Naser, Mjalli, & Gano, 2016). However, to our knowledge, a comprehensive characterization has not been performed.

Quercetin (2-(3,4-dihydroxyphenyl)-3,5,7-trihydroxy-4*H*-chromen-4-one), Q, is a flavonoid with important beneficial applications for health. For instance, it possesses antioxidant, anti-inflammatory and anti-bacterial activities. Studies of its anticancer capacity have also been reported (Wang et al., 2016). Consequently, Q is considered a dietary supplement (Babaei, Mirzababaei, & Nassiri-Asl, 2018) and it is used in industries related to feeding and pharmacology. Many common foods in the human diet (tomatoes and onions, among others) contain quercetin. However, quercetin has major drawbacks due to its extremely low water solubility and its thermal and light instability (Abraham &

Acree, 2014; Zhang et al., 2017). Several authors have determined the solubility of quercetin in organic solvents with the aim of identifying delivery systems to improve its bioavailability (Althans, Schrader, & Enders, 2014; Aytac, Ipek, Durgun, & Uyar, 2016; Buchweitz, Kroon, Rich, & Wilde, 2016; Chen & Yao, 2017; Dai et al., 2013; Kim, Park, Yeo, Choo, & Chong, 2009). Here, we explore the ability of the XoCH and CiCH mixtures to dissolve quercetin.

The present study had two aims: the physicochemical characterization of two aqueous deep eutectic solvents used in the biotechnology industry (xylitol:choline chloride:water (1:2:3) and citric acid:choline chloride:water (1:1:6)) and an assessment of the solubility of a flavonoid (quercetin) in both liquids. Firstly, several NMR spectroscopy experiments allowed us to evaluate the intermolecular interactions between the three components of each DES, establish the role of the water in the mixtures, and calculate the self-diffusion coefficients, D, at 298.15 K. Secondly, seven properties were measured at p=0.1 MPa and at T=(278.15-338.15) K: density, ρ; the speed of sound, u; refraction index, n_D; molar isobaric capacity, $C_{p,m}$; surface tension, γ; kinematic viscosity, ν; and electric conductivity, σ. From these values, we calculated several derived properties, including the isobaric expansion coefficient, α_p; isentropic compressibility, κ_s; intermolecular free length, L_f; free volume, f_m; entropy of the surface, ΔS_S; enthalpy of the surface, ΔH_S; dynamic viscosity, η; and energies of activation for the transport processes, $E_{a,Y}$. Finally, we evaluated the solubility of quercetin in water and in the two DESs.

2. Materials and methods

2.1. Samples

Information about the chemicals used in this work is provided in Table S1 (Supplementary material). All reagents were supplied by Sigma-Aldrich and used without purification, with the exception of choline chloride that was dried under vacuum before utilization. Milli-Q water with a resistivity of less than 18.2 $\mu S \cdot cm^{-1}$ was utilized as the third component. A BP210S Sartorius balance with an uncertainty of 0.1 mg was used to weigh the compounds in adequate proportions: xylitol:choline chloride:water (1:2:3), XoCH, and citric acid:choline chloride:water (1:1:6), CiCH. The water content in percentage by mass was 10.9 and 24.6%, respectively. The two mixtures were obtained by heating the solutions at 323.15 K with magnetic stirring until a colourless and homogeneous liquid formed. Table S2 summarizes the characteristics of the DESs.

2.2. Characterization

2.2.1. NMR spectra

A Bruker AVANCE spectrophotometer operating at 400 MHz and thermosttated at 298 K was used to perform the NMR experiments. The chemical shifts were referenced to tetramethylsilane, TMS, as the standard fluid. For each ^{1}H-NMR spectrum, 8 scans were recorded with a standard one-pulse sequence (Bruker pulse program zg). For each ^{13}C-NMR spectrum, 256 scans were collected with an APT sequence (Bruker pulse program *jmod*). Signal assignation was performed with a routine gradient of selected DQF-COSY, ^{1}H-^{13}C HSQC and ^{1}H-^{13}C HMBC signals (Bruker pulse programs cosygpmfqf, hsqcedetgp and hmbclpndqf, respectively). In addition, Nuclear Overhauser Effect SpectroscopY (NOESY), Rotating-frame Overhauser Effect SpectroscopY (ROESY), and Diffusion-Ordered SpectroscopY (DOSY) experiments were performed

using the pulse programs *noesygpph*, *roesyph*, and *stebpgp1s*, respectively. A more detailed description is provided in the Supplementary Material.

Using the DOSY technique, the self-diffusion coefficients, D, were calculated with the following equation:

$$I(g) = I_0 \exp[-D\gamma_H^2 g^2 \delta^2 (\Delta - \delta/3)] \quad (1)$$

where $I(g)$ is the resonance intensity measured for a given gradient strength, g; I_0 represents the NMR signal in the absence of the gradient pulse; γ_H is the gyromagnetic ratio of the hydrogen nucleus; δ is the duration of the bipolar gradient pulse; and Δ is the observation time.

2.2.2. Thermophysical Properties

Densities, ρ, and speed of sounds, u, were obtained with an Anton Paar DSA 5000 vibrating tube densimeter and sound analyser (3 MHz) that was internally thermostatted to within ± 0.005 K. Dry air and ultrapure water (SH Calibration Service GmbH) were utilized for the calibration. Refractive indices at the sodium D wavelength (589.3 nm), n_D, were measured with an Abbemat-HP refractometer that Dr. Kernchen calibrated with Milli-Q water. The temperature was controlled within ± 0.01 K. A DSC Q2000 calorimeter from TA Instruments with a refrigerated cooling system (RCS) was used to determine the isobaric molar heat capacities, $C_{p,m}$. The zero-heat flow procedure with a sample of synthetic sapphire as a reference system was applied. The surface tension, γ, was measured with a Lauda TVT-2 tensiometer including an external Lauda E-200 thermostat: $u(T)$= ± 0.01 K. Kinematic viscosities, ν, were measured using a Schoot-Geräte AVS-440 automatic measuring unit and several Ubbelohde capillary viscosimeters with different inner diameters. The temperature was controlled with a Schoot-Geräte CT 1150/2 thermostat. The standard uncertainties in the temperature and the time flow were $u(T)$= ± 0.01 K and $u(t)$= ± 0.01 s, respectively. We have calculated

the dynamic viscosity, η, from the density, and kinematic viscosity values, $\eta = \rho \cdot \nu$. Finally, a CRISON conductimeter (model GLP31) with a Lauda E-200 thermostat, $u(T)$= ± 0.01 K, was utilized to measure the electric conductivities, σ. The conductivity cell was calibrated with aqueous KCl solutions supplied by CRISON.

The following combined expanded uncertainties ($k \approx 2$) were calculated for the measured properties: $U_c(\rho)$ = 0.05 kg·m^{-3}; $U_c(u)$ = 0.5 m·s^{-1}; $U_c(n_D)$= 10^{-5}; $U_c(C_{p,m})$= 1 %; $U_c(\gamma)$= 1%; $U_c(\nu)$= 1%; $U_c(\sigma)$= 1%. Several experimental devices were calibrated with cyclohexane (>99.5 %). The measures are reported in the supplementary material (Table S3) and the mean relative deviations between the literature and experimental data, which were calculated using eq. (2), were $MRD(\rho)$ = 0.02%, $MRD(u)$ = 0.9%, $MRD(n_D)$ = 0.02%, $MRD(\eta)$ = 0.99%.

$$MRD(Y) = \frac{100}{n}\sum_{i=1}^{n}\left|\frac{Y_i - Y_{i,exp}}{Y_{i,exp}}\right| \quad (2)$$

where Y_i represents the published or correlated value for the property Y, $Y_{i,exp}$ represents the experimental data, and n represents the number of points.

2.3. Solubility measurements

The thermodynamic solubility was measured with the classic shake-flask method (Baka, 2010). For each study, thermostatted double-walled flasks protected from light with foil were used to perform the experiments. The solid solute was added to approximately 20 ml of solvent in each flask and the heterogeneous system was stirred for several hours at the chosen temperature. Afterwards, the supersaturated solution was sedimented and several aliquots were centrifuged and filtered (PES syringe filter, 0.22 μm). At least six analyses were performed to obtain each result. The concentration of quercetin in the studied solvents was determined using UV-VIS spectroscopy by diluting the mixture in ethanol when necessary. The apparatus was a double-beam spectrum VWR

6300 PC with a wavelength accuracy of ±0.2 nm. Quercetin produces a spectral peak with a maximum absorption, $Abs_{\max}$, of 372-374 nm (Fig. S1a, Supplementary material) that is not influenced by ethanol. A calibration curve (Fig. S1b) was constructed to quantify the mass fraction of dissolved quercetin, W_{q}. The following equation was used

$$Abs_{\max} = 52556.9 \cdot W_{\mathrm{q}} \; ; \; R^2 = 0.9999 \tag{3}$$

3. Results and Discussion

3.1. Structural analysis

3.1.1. XoCH

Fig. S2 shows the ^{1}H-NMR and ^{13}C-NMR spectra of XoCH at 298 K; a description of the chemical shifts is provided in the figure caption. The ^{1}H signals are separated, except for those corresponding to the methylene group bound to the choline nitrogen, CH_2-N^+, the two hydromethylene and central hydroxymethyl groups of xylitol, which overlap. The composition of XoCH obtained from the spectral analysis was a molar ratio of 1:2.02:2.96 of xylitol:choline chloride:water, with an uncertainty of $u(x) = 0.05$. The ^{13}C spectrum presented the expected peaks. By diluting the eutectic in deuterated water (10% DES + 90% D_2O), all the hydrogen aliphatic signals were resolved and the signals for the mobile hydrogens collapsed into the signal for hydrogen-deuterium oxide (Fig. S3a). The shift in the aliphatic signals indicates that the chemical environment has changed substantially and the supramolecular structure has been dissolved. On the other hand, small changes in the ^{13}C signals (Fig. S3b) were observed: +0.3 C_b, +0.2 C_c, +0.3 C_d, +0.5 C_f, +0.7 C_g, +0.4 C_i. Three spectra were recorded at different temperatures (298, 313, and 333 K) to evaluate the effects of changes in both the viscosity and the equilibrium kinetics. No substantial differences were observed, except for an expansion

of the mobile hydrogen signals (Fig. S4). The stability of the eutectic was also checked by recording identical spectra 6 months later (Fig. S5).

NOESY experiments were performed to analyse the interactions between the three components of the mixture. Negative crosspeaks (Fig. 1a) were observed for all intra and intermolecular aliphatic and mobile hydrogens. For the latter hydrogens, we were unable to conclusively determine the nature of the signals, whether they were exclusively derived from chemical exchange or a nOe contribution. Moreover, negative nOes became positive in the ROESY experiment. This result excluded an effect of spin diffusion due to viscosity. In the diluted mixture, no negative nOe was detected (Fig. 1b). However, a positive nOe principally appeared between the choline hydrogens. A representation of the H-H interactions is shown in Fig. 1c.

The mobility of the species can be estimated from DOSY experiments, as described in section 2.2.1. For XoCH, the spectrum showed two traces (Fig. S6a), from which we were able to calculate the self-diffusion coefficients (at 298 K), D, of several species: aliphatic hydrogens of choline, mobile hydrogens of choline, aliphatic hydrogens of xylitol, mobile hydrogens of xylitol, and water. The values are listed in Table 1. For the neat sample, the similarity of D values for the mobile and aliphatic hydrogens of both choline and xylitol and between these two species was remarkable. In addition, water had the highest value, but this value was much lower than the value for free water: $D_{\mathrm{H_2O}}(T=298.15\ \mathrm{K})=230\cdot10^{-11}\ \mathrm{m^2\cdot s^{-1}}$ (Andanson, Traïkia, & Husson, 2014). For the diluted mixture (90% D_2O), the calculated coefficients increased considerably and differed between components. Therefore, the three components were moving separately (Fig. S6b), i.e., the mixtures became an aqueous solution of xylitol and choline chloride.

All results obtained for the neat and diluted mixtures using NMR techniques allowed us to establish the role for the water in the XoCH solvent. Each polar hydrogen

produced an individual signal. NOESY spectra indicated that all molecules behaved as large molecules (negative crosspeaks) due to supramolecular structure and not high viscosity (Delso et al., 2019). Additionally, the different species presented similar diffusivity values. The water did not behave like a solvent; it was located within the supramolecular structure. XoCH was a "water-in-DES" solution (Hammond et al., 2017).

(a) (b)

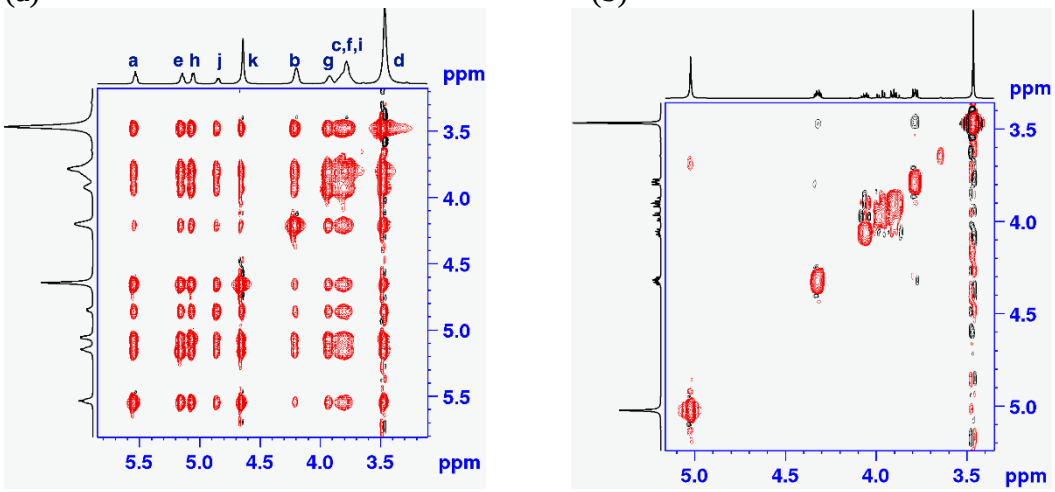

(c)

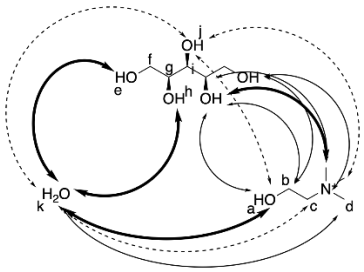

Fig. 1. NOESY spectra recorded at 298 K and t_{mix}=500 ms for (a) neat XoCH and (b) diluted XoCH (10% DES+90% D_2O). (c) Representation of the H-H interactions (thicker lines indicate a stronger interaction).

Table 1.

The diffusion coefficients, D, at 298 K of the following species in the DESs and diluted mixtures (10% DES+90% D_2O)) were obtained: aliphatic hydrogens of choline, Ch^+, mobile hydrogens of choline, $OH-Ch^+$, aliphatic hydrogens of xylitol or citric acid, HBD, mobile hydrogens of xylitol or citric acid, $OH-HBD$, and water, H_2O.

DES	$10^{11}D_{\mathrm{Ch^+}}$ /m^2·s^{-1}	$10^{11}D_{\mathrm{OH-Ch^+}}$ /m^2·s^{-1}	$10^{11}D_{HBD}$ /m^2·s^{-1}	$10^{11}D_{\mathrm{OH}-HBD}$ /m^2·s^{-1}	$10^{11}D_{\mathrm{H_2O}}$ /m^2·s^{-1}
XoCH	0.584	0.648	0.549	4.77[a]	4.39
Diluted XoCH	70.5	---	52.4	---	174
CiCH	1.73	---	1.22		11.9
Diluted CiCH	69.9	---	46.7	---	173

3.1.2. CiCH

For CiCH, all signals corresponding to the aliphatic hydrogens were separate, whereas the signals for mobile hydrogens appeared in a single peak (Fig. S7a). Following integration, the composition of CiCH reported as a molar ratio was1.01:1:6.05 citric acid:choline chloride:water; ($u(x)$ =0.05). The ^{13}C-NMR spectrum (Fig. S7b) displayed the expected signals. The chemical shifts for both spectra are described in the figure captions.

For diluted CiCH (90% D_2O), the resolution of ^{1}H-NMR spectrum (Fig. S8a) increased and the hydrogen-deuterium oxide signal was significantly displaced. However, very little change in the aliphatic peaks was observed, indicating that the chemical environment had not changed substantially following dilution. Additionally, substantial changes in the ^{13}C signals were not observed (Fig. S8b): +0.3 C_b, +0.3 C_c, +0.1 C_d, -0.6 C_e, 0.0 C_g, and -0.5 C_h.

NOESY spectra of neat and diluted CiCH mixtures are presented in Fig. 2a and 2b, respectively. In the neat sample, only positive signals corresponding to the intramolecular interactions and intermolecular crosspeaks between water and methyl groups in choline were detected. On the other hand, no intermolecular signals were observed for the diluted CiCH.

The diffusion coefficients for choline, citric acid, and water in neat and diluted CiCH mixtures (Table 1) were calculated from DOSY experiments (Fig. S9) using eq. 1. A single trace displayed all hydrogens (aliphatic and mobile) for each component. In CiCH, choline and citric acid had similar diffusivity values, while water displayed faster diffusion. Following dilution, the differences in mobility increased significantly and D_{H_2O} values for diluted XoCH and CiCH samples were similar.

Based on these findings, CiCH was a "DES-in-water" system, in contrast to the mixture containing xylitol (Hammond et al., 2017).

(a) (b)

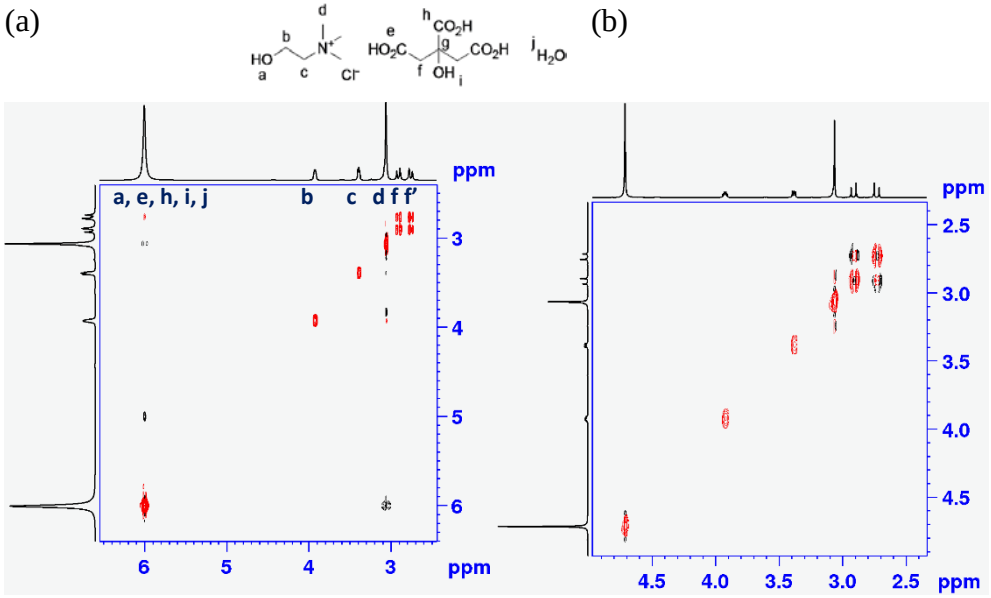

Fig. 2. NOESY spectra (t_{mix}=500 ms) recorded at 298 K for (a) neat CiCH and (b) diluted CiCH (10% DES+90% D_2O).

3.2.Thermophysical study

3.2.1. Thermodynamic properties

Tables S4 and S5 report the values of the thermodynamic properties determined in the present study. The properties include the density, ρ, speed of sound, u, refractive index, n_D, and isobaric molar heat capacity, $C_{p,m}$. The measurements were performed at

p = 0.1 MPa and T = 283.15 – 338.15 K with intervals of 2.5 K. For n_D, the temperature ranged from 283.15 to 338.15 K.

A linear relationship between these properties and the temperature, T, was observed:

$$Y = A_Y + B_Y \cdot T \quad (4)$$

where Y is the property and T is the temperature in kelvin. The A_Y and B_Y coefficients are the fit parameters whose values are listed in Table 2.

Table 2.

Fitting parameters for the thermophysical properties of the studied DESs. Regression coefficients for the linear fitting (eq. 4), R^2, and mean relative deviations, MRD (eq. 2), for the exponential fits (eqs. 11 and 12) are included.

DES	Property	A_Y	B_Y	C_Y	R^2/MRD
XoCH	ρ / kg·m^{-3}	1342.63	-0.527		1.0000
	u / m·s^{-1}	2777.04	-2.217		0.9998
	n_D	1.55472	-2.25·10^{-4}		1.0000
	$C_{p,m}$ / J·mol·K^{-1}	109.70	0.274		0.9995
	γ / mN·m^{-1}	126.57	-0.165		0.9979
	η [a] / mPa·s	0.0462	1167.19	160.74	0.64%
	σ [b] / mS·cm^{-1}	2905.29	849.23	174.59	0.40%
CiCH	ρ / kg·m^{-3}	1434.26	-0.631		1.0000
	u / m·s^{-1}	2410.16	-1.758		0.9998
	n_D	1.52599	-2.39·10^{-4}		1.0000
	$C_{p,m}$ / J·mol·K^{-1}	68.62	0.215		0.9998
	γ / mN·m^{-1}	98.21	-0.099		0.9979
	η [a] / mPa·s	0.0670	938.86	164.57	0.40%
	σ [b] / mS·cm^{-1}	1060.30	636.36	177.15	0.90%

277 $^{a}A_{\eta}$ /mPa·s = η_{∞}; $^{b}A_{\sigma}$ /mS·cm^{-1} = σ_{∞}

278 The measured densities were higher than most other eco-friendly solvents, such
279 as sc-CO_2 or bio-based liquids, and similar to other choline chloride-based DESs (Pena-
280 Pereira et al., 2015). At 298.15 K, the values for XoCH and CiCH were 1185.37 and
281 1245.98 kg·m^{-3}, respectively. In the range of studied temperatures, CiCH was
282 approximately 5% denser than XoCH. For the DES with xylitol, we have only identified
283 the density data at 313.15 K published by Dai et al. (Dai et al., 2013). The data were
284 consistent, and the calculated deviation (eq. 2) was MRD=0.07%. For the DES with citric
285 acid, we obtained some values for mixtures with different water contents, W. Craveiro et
286 al. (Craveiro et al., 2016) published the density at 296 K and W=0.2% wt of ρ=1.30·10^{3}
287 kg·m^{-3}. At 318.15 K and W=1.431% wt, the value reported by Altamash et al. (Altamash
288 et al., 2017) was ρ=1308.9 kg·m^{-3}. Finally, Tang et al. (Tang et al., 2016) have published
289 densities at temperatures ranging from 293.15 to 323.15 K for a mixture containing
290 37.37% wt of water. The temperatures at which the data published by Crespo et al. were
291 recorded (Crespo et al., 2018) are higher than the temperatures used in our experiments.
292 A comparison with our results is displayed in Fig. S10a, in which a decrease in density
293 as the water content increased was observed. On the other hand, the density of the {citric
294 acid+water} binary mixture with a similar acid content to CiCH recorded at 298.15 K was
295 approximately 4.5% lower (Żarska, Dzida, & Apelblat, 2017). Therefore, the addition of
296 choline chloride increased the ρ value. An increase in the thermal agitation weakens the
297 interactions. Consequently, the density of the liquid is lower at higher temperatures. This
298 variation is shown in Fig. 3a, and the effect was quantified with the isobaric expansion
299 coefficient, α_p, calculated using the following equation:

$$\alpha_p = -\frac{1}{\rho}\left(\frac{\partial \rho}{\partial T}\right)_p \quad (5)$$

The α_p values ranged from 0.441 to 0.453 (±0.04) kK^{-1} for XoCH and from 0.502 to 0.518 (±0.05) kK^{-1} for CiCH. The larger calculated value for α_p, i.e., greater expansion capacity, indicated that the DES with citric acid had lower intermolecular forces.

High values for the speed of sound, u, were determined for both systems (Tables S4 and S5). In fact, the values for XoCH were at the upper limit of the measuring range of the apparatus. At 298.15 K, u=2115.05 and 1885.93 $m \cdot s^{-1}$ for XoCH and CiCH, respectively. Because sound is propagated through an elastic medium, sound waves travel faster in a more compact material. Therefore, these solvents are fluids with compact packaging. Based on the ρ and u values, we calculated the isentropic compressibility, κ_S, and the intermolecular free length from the Jacobson relation (Jacobson, 1952), L_f:

$$\kappa_S = \frac{1}{\rho u^2} \tag{6}$$

$$L_f = K\sqrt{\kappa_S} \tag{7}$$

where K=(91.368+0.3565T)10^{-8} is the temperature-dependent Jacobson's constant. For the XoCH mixture, the calculated values of κ_S were ranged from 178.73 – 208.84 (±0.05) TPa^{-1}, whereas the values for CiCH ranged from 215.29 to 249.35 (±0.05) TPa^{-1}. Thus, the solvent containing xylitol was the most compact; L_f for CiCH was approximately 10% higher (Table S6). Logically, the packing decreases and hence u decreases as the temperature increases (Fig. 3b).

The refractive index, n_D, is related to the electronic molecular polarizability, α_e, that in turn is proportional to the forces of intermolecular dispersion. Therefore, light waves travel more slowly in a more compact material. According to the results presented above, smaller n_D values were obtained for CiCH that decreased as T increased (Fig. 3c). We calculated the molar refraction, R_m, from the ρ and n_D values using the Lorentz-Lorenz relation:

$$R_m = \frac{N_A \alpha_e}{3\varepsilon_0} = \frac{M \cdot (n_D^2 - 1)}{\rho \cdot (n_D^2 + 2)} \quad (8)$$

where M is the molar mass calculated from the molar ratio of each component, i: $M = \sum_i M_i x_i$. A solvent with a greater electronic polarizability exhibits a greater ability to dissolve highly polarizable compounds. The pronounced difference in R_m between both DESs (Table S6) shows that XoCH has stronger dispersion forces than CiCH. Thus, a greater solubility in the first DES would be predicted. The free volume, f_m, was calculated by subtracting the molar volume from the molar refraction. Higher values (Table S6) were obtained for the DES with xylitol, but the f_m/V_m ratio was smaller. At 298.15 K, the estimated percentages of free volume were 71.2 and 72.9% for XoCH and CiCH, respectively.

The isobaric molar heat capacity, $C_{p,m}$, of the fluids must be calculated for processes involving energy transfer. This property depends of the number of motion degrees of freedom in the system that vary with the number of inter- and intramolecular bonds. The calculated values for XoCH were higher (approximately 30% at 298.15 K), consistent with the results presented above indicating stronger interactions within the liquid. For both DESs, $C_{p,m}$ increased with temperature (Fig. 3d), showing similar behaviours to other solvents, such as ILs (Bandrés, Giner, Artigas, Royo, & Lafuente, 2008). No phase changes were detected in the calorimetric scan. The glass transition temperature measured by Dai et al. (Dai et al., 2013) for XoCH was T_g=179.82 K. The melting point for CiCH has not been reported in the literature. Naser et al. (Naser et al., 2016) measured the $C_{p,m}$ of DESs formed from a quaternary ammonium salt such as HBA and several donors, including citric acid. However, the molar ratio was not the same as in our DESs.

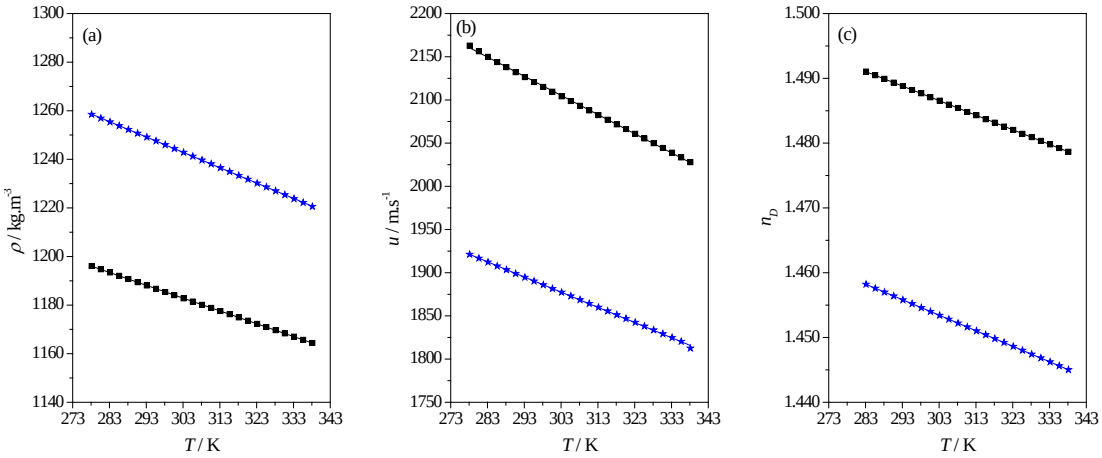
(a)
ρ / kg.m-3
T / K
(b)
u / m.s-1
T / K
(c)
nD
T / K

344

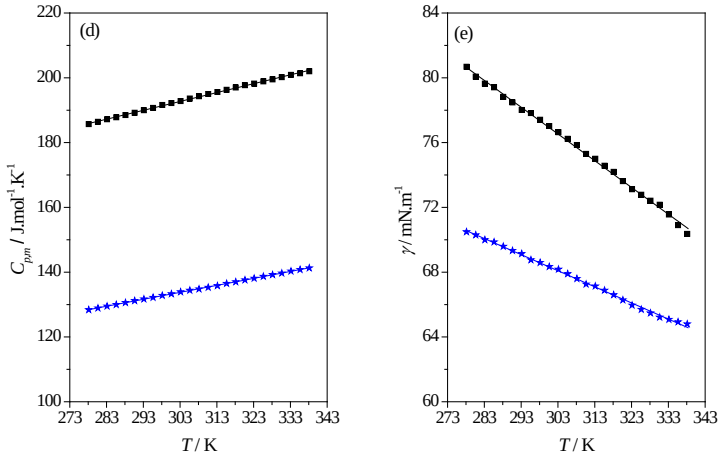
(d)
Cpm / J.mol-1.K-1
T / K
(e)
γ / mN.m-1
T / K

345

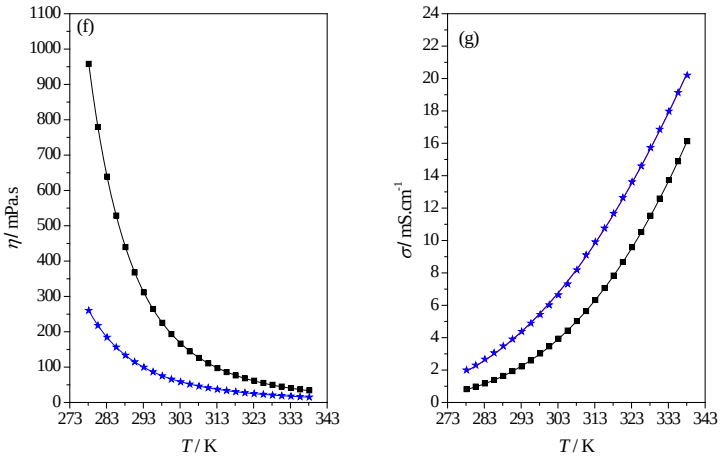
(f)
η / mPa.s
T / K
(g)
σ / mS.cm-1
T / K

346

Fig. 3. Thermophysical properties of the studied DESs: (■) XoCH and (★) CiCH. (a) Density, ρ; (b) speed of sound, u; (c), refractive index, n_D; (d), isobaric molar heat capacity, $C_{p,m}$; (e) surface tension, γ; (f) dynamic viscosity, η; and (g) electric conductivity, σ. Points represent experimental values and lines represent correlated data (eqs. 4, 11, and 12).

The chemical environment of a molecule inside a liquid differs from its environment when it is located on the surface of an interface. In the bulk solution, the molecule is subjected to the cohesion forces, whereas on the surface, it is influenced by the adhesion forces. The difference between both types of forces is the origin of the surface tension, γ. Based on the results presented above, the γ values of both DESs are expected to be large and XoCH will present the highest values; these data are reported in Tables S4 and S5. The positive effect exerted by fluids with high γ values on the stabilization of proteins has been reported in the literature (Kaushik & Bhat, 1998). The values for our mixtures were particularly high. The value for XoCH was even greater than water (Romero & Albis, 2010). At 298.15 K, γ(XoCH)= 77.41 mN·m^{-1} and γ(CiCH)= 68.59 mN·m^{-1}. Moreover, γ(CiCH) values were higher than the values for an aqueous acid solution with a similar mass fraction (Żarska et al., 2017). Thus, the replacement of water with choline chloride increases intermolecular interactions. For XoCH, this comparison is not possible. We have not found γ values for aqueous mixtures with xylitol and an analogous composition to the mixture studied here in the literature. A linear decrease in this value with the temperature was also observed (Fig. 3e), and the fit coefficients (eq. 4) are reported in Table 2. Two thermodynamic functions, the entropy and the enthalpy of the surface per unit surface area (ΔS_S and ΔH_S), were calculated from γ values to determine the effect of the temperature:

$$\Delta S_S = -(\partial\gamma/\partial T)_p \quad (9)$$

$$\Delta H_S = \gamma - T(\partial\gamma/\partial T)_p \quad (10)$$

ΔS_S indicates a change in the order of the molecules when the interface is formed. Because γ was a linear function of the temperature, ΔS_S was constant for each mixture: 0.1651 (±0.002) and 0.0994 (±0.001) mN·m^{-1}·K^{-1} for XoCH and CiCH, respectively. At 298.15 K, the enthalpies of the surface calculated for XoCH and CiCH were $\Delta H_S = 126.5$ and 98.2 mN·m^{-1}, respectively. The high values for the thermodynamic properties of the surface calculated for these aqueous DESs confirmed that they are very structured liquids. As deduced from the spectroscopic and thermodynamic data, XoCH possessed the strongest cohesive forces.

3.2.2. Transport properties

In this section, both the fluidity and the electric mobility were evaluated from two interrelated transport properties: dynamic viscosity, η, and the electric conductivity, σ. The measurements were performed at p = 0.1 MPa, and at T = 278.15 – 338.15 K with intervals of 2.5 K, and the values are listed in Tables S4 and S5.

In general, DESs are characterized by a much higher viscosity than other solvents (Pena-Pereira et al., 2015). These values are impractical in the most of the industrial operations and are related to both the size of the species and the H-bond network established within the liquid. The inclusion of water in the composition of the eutectic allows the fluidity of the liquid to be modulated. At 293 K, the viscosity of the non-aqueous choline chloride:citric acid (1:1) eutectic is 10224 Pa·s (Aroso et al., 2017); the addition of 24.6% wt of water (this study) results in η= 99.51 mPa·s, and the addition of 37.4% wt of water results in η= 15.842 mPa·s (Tang et al., 2016). Fig. S10b shows the changes in viscosity at several temperatures and water contents. The non-aqueous DES containing xylitol was not a liquid at room temperature, and viscosity data have not been

reported. On the other hand, Dai et al. (Dai et al., 2013) measured the viscosity of XoCH at 313 K, and the published value is slightly lower than the value reported in the present study. As calculated with eq. 2, the small deviation between the two values, $MRD(\eta)$= 4.7%, may be due to the marginally higher water content in their mixture (11.17% wt). The greater difference in viscosity observed for the two studied mixtures was basically attributed to the difference in water content; CiCH had a two-fold higher water content than XoCH.

Regarding the electric conductivity, σ, the measured values, up to 20.20 mS·cm, were higher for the CiCH mixture due to its higher mobility (Tables S4 and S5). The conductivity of this system at different temperatures and water contents is displayed in Fig. S10c. An increase in the water content increased the conductivity as consequence of the effect on the viscosity.

Due to the effect of the temperature on the intermolecular interactions, the movement of species within the fluid is favoured at higher *T*. The effect of temperature is more pronounced at lower *T*. Therefore, η decreases and σ increases exponentially with increasing *T* (Fig. 3f and 3g). Specifically, we used the Vogel-Fulcher-Tammann (VFT) equation to calculate the values of these parameters:

$$\eta = A_\eta \cdot \exp\left(\frac{B_\eta}{T - C_\eta}\right) \tag{11}$$

$$\sigma = A_\sigma \cdot \exp\left(-\frac{B_\sigma}{T - C_\sigma}\right) \tag{12}$$

where *T* is the temperature in kelvin and A_Y, B_Y, and C_Y are the fit parameters (Table 2). A_Y is the value of the property *Y* at infinite temperature when the intermolecular interactions are negligible, i.e., the only factors that contribute to the transport property are the size and shape of the molecules. On the other hand, B_Y and C_Y are related to the

energy barrier that must be overcome for transport, $E_{a,Y}$, and are calculated using the following equation:

$$E_{a,Y} = R \cdot \frac{\partial(lnY)}{\partial\left(\frac{1}{T}\right)} = R \cdot \left(\frac{B_Y}{\left(\frac{C_Y^2}{T^2} - \frac{2C_Y}{T} + 1\right)} \right) \quad (13)$$

For XoCH, the calculated values of $E_{a,\eta}$ and $E_{a,\sigma}$ were 45.69 and 41.14 kJ·mol^{-1}, respectively. For CiCH, $E_{a,\eta}$= 38.89 kJ·mol^{-1} and $E_{a,\sigma}$= 32.12 kJ·mol^{-1}. Thus, the A_η parameter for XoCH was lower than CiCH, whereas $E_{a,Y}$ was higher. Based on this results, the steric hindrance was greater in the mixture with citric acid, but the interactions were stronger in the mixture containing xylitol, consistent with the discussion above. Fig. S11 displays the relationship between $E_{a,\sigma}$ and $E_{a,\eta}$ for CiCH mixtures with different water contents. Our results are consistent with data reported in the literature (Aroso et al., 2017). A good linear proportionality (R^2= 0.98) between the energies involved in both transport phenomena was obtained.

3.3. Quercetin solubility

Differences in the experimental procedure (protecting or exposing the vessels to light or the type of filter) result in a disparity between the values measured because of the low solubility of quercetin in water. Fig. 4 shows the wide distribution of data reported in the literature; the solubility is presented as log C_q for a better comparison. Using the procedure described in section 2.3, we determined the solubility at 298.15 K. The average value (in mass fraction) obtained, $W_q(H_2O)$= 4.3·10^{-7}, was very similar to the value published by Althans et al. (Althans et al., 2014). As mentioned in the introduction, both the solubility and the permeability through membranes of drugs/nutraceuticals with poor water solubility increase when mixed with DESs as a vehicle. Thus, the substitution of

aqueous media with DES in the biotechnological industry potentially represent a viable strategy to increase the bioavailability of these compounds.

Fig. 4 shows the solubility of quercetin at 298.15 K in the studied mixtures, and the values were W_q(XoCH)= $2.22 \cdot 10^{-2}$ and W_q(CiCH)= $3.22 \cdot 10^{-4}$, respectively. Only one study (Dai et al., 2013) reported the value for quercetin solubility in XoCH at 313.15 K (W_q= 0.608), which, as expected, is greater than the value reported in the present study due to the higher T. The remarkable increase in solubility compared to water (5 and 3 orders of magnitude) may be related to the presence of the H-bond network that favours the dissolution process and stabilizes the system. A stronger H-bond network results in a higher solubility. We have determined the solubility of quercetin in the xylitol:choline chloride (1:2) mixture with a similar water content to CiCH (24.6%) to confirm the effect of water. The value measured, $9.93 \cdot 10^{-4}$, was much lower than XoCH. This result is consistent with the observation that the presence of water weakens the H-bond network in the DESs(Delso et al., 2019; Hammond et al., 2017). We also concluded that the interactions between choline chloride and xylitol were stronger than the interactions with citric acid because the solubility value was 3-fold higher than for CiCH. Therefore, both studied DESs are potentially useful as effective flavonoid solvents, but XoCH to a greater extent. Only one published study has reported (Dai et al., 2013) the value for quercetin solubility in XoCH at 313.15 K (W_q= 0.608), which, as expected, is greater than the value reported in the present study due to the higher T. Tang et al. (Tang et al., 2016) measured the solubility of three flavonoids (phloretin, phlorizin, and naringin) in the following DESs: citric acid:glucose:water (1:1:12), choline chloride:glucose:water (1:1:11), choline chloride:sucrose:water (1:1:10), and citric acid:choline chloride:water (1:1:11). A considerable increase in solubility was observed in the two latter mixtures. Additionally,

Zhao et al. (Zhao et al., 2015) studied the potential use of DESs as green solvents for the extraction of rutin.

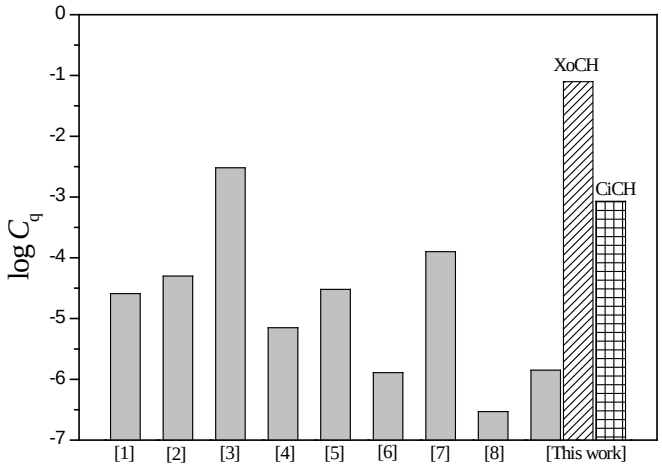

Fig. 4. Solubility of quercetin in water (■) and in the studied DESs at T= 298.15 K. [1] (Lauro, M.R.; Torre, M.L., Maggi, L., De Simone, F., Conte, U., Aquino, 2002); [2] (Kim et al., 2009); [3] (Razmara, Daneshfar, & Sahraei, 2010); [4] (Srinivas, King, Howard, & Monrad, 2010); [5] (Chebil et al., 2010); [6] (Althans et al., 2014); [7] (Abraham & Acree, 2014); [8] (Zhang et al., 2017)

The intermolecular interactions among the flavonoid and the DES components in both solutions were elucidated using NMR. However, only the sample in XoCH had a quercetin concentration that was sufficiently high to be detected in the presence of the non-deuterated DES (Figs. S12 and S13). By integrating the signals in the ^{1}H-NMR spectrum, we were able to calculate the quercetin concentration in the choline chloride:quercetin molar ratio of 1:0.0175 with an uncertainty $u(x) = 0.0006$ using the data presented above. NOESY experiments revealed many intermolecular interactions between quercetin and the three components of XoCH. After short mixing times (50 ms), highest crosspeaks corresponded to mobile protons that were presumably derived from chemical exchange and intramolecular crosspeaks in quercetin (Fig. S14a). When the

mixing time increased to 500 ms, no intramolecular crosspeaks were observed for quercetin, but crosspeaks for intramolecular interactions of aliphatic hydrogens between quercetin and DES components were detected (Fig. S14b). After a more careful analysis of the crosspeak intensities (excluding exchanging OH signals), we were able to identify signals arising from water-quercetin aliphatic protons as the most intense crosspeaks, followed by choline methyl groups. These signals suggest a strong interaction between the solute and the solvent, and unexpectedly, water appears to play an important role in this interaction, possibly by favouring an environment rich in hydrogen bonds.

4. Conclusions

Two deep eutectic solvents (DESs) containing water were characterized in the present study. The structure was evaluated using several NMR spectroscopy techniques: ^{1}H and ^{13}C, COSY, HSQC, NOESY, ROESY, and DOSY. Moreover, the following thermodynamic, surface and transport properties were measured and discussed: density, ρ; speed of sound, u; refraction index, n_D; molar isobaric capacity, $C_{p,m}$; surface tension, γ; kinematic viscosity, ν; and electric conductivity, σ. Other derived properties were calculated from the experimental data. Finally, the thermodynamic solubility of quercetin in water, XoCH, and CiCH was determined. The results obtained from both the spectroscopic experiments and the thermophysical properties revealed that XoCH displays the most compact structure.

NMR results for the neat XoCH and a more diluted mixture revealed the formation of a supramolecular structure between xylitol, choline chloride and water molecules. On the other hand, a similar study confirmed that CiCH was an aqueous solution of DES. Of the thermophysical properties, the high values measured for the speed of sound, surface tension, and viscosity are worth noting. We observed a greater steric hindrance in CiCH

and stronger intermolecular interactions in XoCH. Regarding the solubility of quercetin, we concluded that the solubility of this flavonoid was remarkably increased in the characterized DESs. The $W_q(\mathrm{DES})/W_q(\mathrm{H_2O})$ ratio was $5{\cdot}10^4$ for XoCH and $7{\cdot}10^2$ for CiCH.

Supplementary data

Supplementary data accompanying this article can be found in the online version.

Declaration of interests

Non-declared.

Acknowledgments

This research was supported by Gobierno de Aragón (Grant E31_17R), Fondo de Desarrollo Regional "Construyendo Europa desde Aragón". The authors would like to thank the financial assistance.

References

Abbott, A. P., Boothby, D., Capper, G., Davies, D. L., & Rasheed, R. K. (2004). Deep Eutectic Solvents formed between choline chloride and carboxylic acids: Versatile alternatives to ionic liquids. *Journal of the American Chemical Society*, *126*(29), 9142–9147. https://doi.org/10.1021/ja048266j

Abraham, M. H., & Acree, W. E. (2014). On the solubility of quercetin. *Journal of Molecular Liquids*, *197*, 157–159. https://doi.org/10.1016/j.molliq.2014.05.006

Altamash, T., Nasser, M. S., Elhamarnah, Y., Magzoub, M., Ullah, R., Anaya, B., … Atilhan, M. (2017). Gas Solubility and Rheological Behavior of Natural Deep

524 Eutectic Solvents (NADES) via Combined Experimental and Molecular
525 Simulation Techniques. *ChemistrySelect*, *2*(24), 7278–7295.
526 https://doi.org/10.1002/slct.201701223
527 Althans, D., Schrader, P., & Enders, S. (2014). Solubilisation of quercetin: Comparison
528 of hyperbranched polymer and hydrogel. *Journal of Molecular Liquids*, *196*, 86–
529 93. https://doi.org/10.1016/j.molliq.2014.03.028
530 Andanson, J., Traïkia, M., & Husson, P. (2014). Ionic association and interactions in
531 aqueous methylsulfate alkyl-imidazolium-based ionic liquids. *The Journal of*
532 *Chemical Thermodynamics*, *77*, 214–221. https://doi.org/10.1016/j.jct.2014.01.031
533 Aroso, I. M., Paiva, A., Reis, R. L., & Duarte, A. R. C. (2017). Natural deep eutectic
534 solvents from choline chloride and betaine – Physicochemical properties. *Journal*
535 *of Molecular Liquids*, *241*, 654–661. https://doi.org/10.1016/j.molliq.2017.06.051
536 Aytac, Z., Ipek, S., Durgun, E., & Uyar, T. (2016). Quercetin / b -cyclodextrin inclusion
537 complex embedded nanofibres : Slow release and high solubility. *Food Chemistry*,
538 *197*, 864–871. https://doi.org/10.1016/j.foodchem.2015.11.051
539 Babaei, F., Mirzababaei, M., & Nassiri-Asl, M. (2018). Quercetin in Food: Possible
540 Mechanisms of Its Effect on Memory. *Journal of Food Science*, *83*(9), 2280–2287.
541 https://doi.org/10.1111/1750-3841.14317
542 Bajkacz, S., & Adamek, J. (2018). Development of a Method Based on Natural Deep
543 Eutectic Solvents for Extraction of Flavonoids from Food Samples. *Food*
544 *Analytical Methods*, *11*(5), 1330–1344. https://doi.org/10.1007/s12161-017-1118-5
545 Baka, E. (2010). *Development and examination of solubility measurement methods for*
546 *drug solubility determination*. Smmelweis University, Budapest.
547 Bandrés, I., Giner, B., Artigas, H., Royo, F. M., & Lafuente, C. (2008). Thermophysic
548 Comparative Study of Two Isomeric Pyridinium-Based Ionic Liquids. *The Journal*

549 *of Physical Chemistry B*, *112*(10), 3077–3084. https://doi.org/10.1021/jp077259p
550 Bosiljkov, T., Dujmić, F., Cvjetko Bubalo, M., Hribar, J., Vidrih, R., Brnčić, M., …
551 Jokić, S. (2017). Natural deep eutectic solvents and ultrasound-assisted extraction:
552 Green approaches for extraction of wine lees anthocyanins. *Food and Bioproducts*
553 *Processing*, *102*, 195–203. https://doi.org/10.1016/j.fbp.2016.12.005
554 Buchweitz, M., Kroon, P. A., Rich, G. T., & Wilde, P. J. (2016). Quercetin
555 solubilisation in bile salts : A comparison with sodium dodecyl sulphate. *Food*
556 *Chemistry*, *211*, 356–364. https://doi.org/10.1016/j.foodchem.2016.05.034
557 Chebil, L., Chipot, C., Archambault, F., Humeau, C., Engasser, J. M., Ghoul, M., … V,
558 N. U. (2010). Solubilities Inferred from the Combination of Experiment and
559 Simulation . Case Study of Quercetin in a Variety of Solvents, 12308–12313.
560 Chen, H., & Yao, Y. (2017). Phytoglycogen improves the water solubility and Caco-2
561 monolayer permeation of quercetin. *Food Chemistry*, *221*, 248–257.
562 https://doi.org/10.1016/j.foodchem.2016.10.064
563 Clarke, C. J., Tu, W. C., Levers, O., Bröhl, A., & Hallett, J. P. (2018). Green and
564 Sustainable Solvents in Chemical Processes. *Chemical Reviews*, *118*(2), 747–800.
565 https://doi.org/10.1021/acs.chemrev.7b00571
566 Craveiro, R., Aroso, I., Flammia, V., Carvalho, T., Viciosa, M. T., Dionísio, M., …
567 Paiva, A. (2016). Properties and thermal behavior of natural deep eutectic solvents.
568 *Journal of Molecular Liquids*, *215*, 534–540.
569 https://doi.org/10.1016/j.molliq.2016.01.038
570 Crespo, E. A., Silva, L. P., Martins, M. A. R., Bülow, M., Ferreira, O., Sadowski, G., …
571 Coutinho, J. A. P. (2018). The Role of Polyfunctionality in the Formation of
572 [Ch]Cl-Carboxylic Acid-Based Deep Eutectic Solvents. *Industrial and*
573 *Engineering Chemistry Research*, *57*(32), 11195–11209.

https://doi.org/10.1021/acs.iecr.8b01249

Dai, Y., van Spronsen, J., Witkamp, G. J., Verpoorte, R., & Choi, Y. H. (2013). Natural deep eutectic solvents as new potential media for green technology. *Analytica Chimica Acta*, *766*, 61–68. https://doi.org/10.1016/j.aca.2012.12.019

Dai, Y., Witkamp, G. J., Verpoorte, R., & Choi, Y. H. (2015). Tailoring properties of natural deep eutectic solvents with water to facilitate their applications. *Food Chemistry*, *187*, 14–19. https://doi.org/10.1016/j.foodchem.2015.03.123

Delso, I., Lafuente, C., Muñoz-Embid, J., & Artal, M. (2019). NMR study of choline chloride-based deep eutectic solvents. *Journal of Molecular Liquids*, *290*, 111236. https://doi.org/10.1016/j.molliq.2019.111236

Deng, W., Yu, L., Li, X., Chen, J., Wang, X., Deng, Z., & Xiao, Y. (2019). Hexafluoroisopropanol-based hydrophobic deep eutectic solvents for dispersive liquid-liquid microextraction of pyrethroids in tea beverages and fruit juices. *Food Chemistry*, *274*(September 2018), 891–899. https://doi.org/10.1016/j.foodchem.2018.09.048

Espino, M., de los Ángeles Fernández, M., Gomez, F. J. V., & Silva, M. F. (2016). Natural designer solvents for greening analytical chemistry. *TrAC - Trends in Analytical Chemistry*, *76*, 126–136. https://doi.org/10.1016/j.trac.2015.11.006

García, A., Rodríguez-Juan, E., Rodríguez-Gutiérrez, G., Rios, J. J., & Fernández-Bolaños, J. (2016). Extraction of phenolic compounds from virgin olive oil by deep eutectic solvents (DESs). *Food Chemistry*, *197*, 554–561. https://doi.org/10.1016/j.foodchem.2015.10.131

González, C. G., Mustafa, N. R., Wilson, E. G., Verpoorte, R., & Choi, Y. H. (2018). Application of natural deep eutectic solvents for the “green”extraction of vanillin from vanilla pods. *Flavour and Fragrance Journal*, *33*(1), 91–96.

https://doi.org/10.1002/ffj.3425

Hammond, O. S., Bowron, D. T., & Edler, K. J. (2017). The Effect of Water upon Deep Eutectic Solvent Nanostructure: An Unusual Transition from Ionic Mixture to Aqueous Solution. *Angewandte Chemie - International Edition*, *56*(33), 9782–9785. https://doi.org/10.1002/anie.201702486

Huang, Y., Feng, F., Chen, Z. G., Wu, T., & Wang, Z. H. (2018). Green and efficient removal of cadmium from rice flour using natural deep eutectic solvents. *Food Chemistry*, *244*(September 2017), 260–265. https://doi.org/10.1016/j.foodchem.2017.10.060

Jacobson, B. (1952). Ultrasonic Velocity in Liquids and Liquid Mixtures. *The Journal of Chemical Physics*, *20*(5), 927–928. https://doi.org/10.1063/1.1700615

Kaushik, J. K., & Bhat, R. (1998). Thermal Stability of Proteins in Aqueous Polyol Solutions: Role of the Surface Tension of Water in the Stabilizing Effect of Polyols. *The Journal of Physical Chemistry B*, *102*(36), 7058–7066. https://doi.org/10.1021/jp981119l

Kim, M. K., Park, K. su, Yeo, W. seok, Choo, H., & Chong, Y. (2009). In vitro solubility, stability and permeability of novel quercetin-amino acid conjugates. *Bioorganic and Medicinal Chemistry*, *17*(3), 1164–1171. https://doi.org/10.1016/j.bmc.2008.12.043

Lapeña, D., Lomba, L., Artal, M., Lafuente, C., & Giner, B. (2019). The NADES glyceline as a potential Green Solvent: A comprehensive study of its thermophysical properties and effect of water inclusion. *The Journal of Chemical Thermodynamics*, *128*, 164–172. https://doi.org/10.1016/j.jct.2018.07.031

Lauro, M.R.; Torre, M.L., Maggi, L., De Simone, F., Conte, U., Aquino, R. P. (2002). Fast- and slow-release tablets for oral administration of flavonoids: Rutin and

624 quercetin. *Drug Dev. Ind. Pharm*, *28*, 371–379. https://doi.org/10.1081/DDC-
625 120002998
626 Liu, Y., Friesen, J. B., McAlpine, J. B., Lankin, D. C., Chen, S. N., & Pauli, G. F.
627 (2018). Natural Deep Eutectic Solvents: Properties, Applications, and Perspectives.
628 *Journal of Natural Products*, *81*(3), 679–690.
629 https://doi.org/10.1021/acs.jnatprod.7b00945
630 Lores, H., Romero, V., Costas, I., Bendicho, C., & Lavilla, I. (2017). Natural deep
631 eutectic solvents in combination with ultrasonic energy as a green approach for
632 solubilisation of proteins: application to gluten determination by immunoassay.
633 *Talanta*, *162*(June 2016), 453–459. https://doi.org/10.1016/j.talanta.2016.10.078
634 Martins, M. A. R., Pinho, S. P., & Coutinho, J. A. P. (2018). Insights into the Nature of
635 Eutectic and Deep Eutectic Mixtures. *Journal of Solution Chemistry*, (August).
636 https://doi.org/10.1007/s10953-018-0793-1
637 Maugeri, Z., & Domínguez De María, P. (2012). Novel choline-chloride-based deep-
638 eutectic-solvents with renewable hydrogen bond donors: Levulinic acid and sugar-
639 based polyols. *RSC Advances*, *2*(2), 421–425. https://doi.org/10.1039/c1ra00630d
640 Naser, J., Mjalli, F. S., & Gano, Z. S. (2016). Molar Heat Capacity of Selected Type III
641 Deep Eutectic Solvents. *Journal of Chemical and Engineering Data*, *61*(4), 1608–
642 1615. https://doi.org/10.1021/acs.jced.5b00989
643 Pena-Pereira, F., Kloskowski, A., & Namieśnik, J. (2015). Perspectives on the
644 replacement of harmful organic solvents in analytical methodologies: A framework
645 toward the implementation of a generation of eco-friendly alternatives. *Green*
646 *Chemistry*, *17*(7), 3687–3705. https://doi.org/10.1039/c5gc00611b
647 Posada, E., López-Salas, N., Jiménez Riobóo, R. J., Ferrer, M. L., Gutiérrez, M. C., &
648 del Monte, F. (2017). Reline aqueous solutions behaving as liquid mixtures of H-

649 bonded co-solvents: microphase segregation and formation of co-continuous
650 structures as indicated by Brillouin and 1 H NMR spectroscopies. *Physical*
651 *Chemistry Chemical Physics*, *19*(26), 17103–17110.
652 https://doi.org/10.1039/C7CP02180A
653 Razmara, R. S., Daneshfar, A., & Sahraei, R. (2010). Solubility of Quercetin in Water +
654 Methanol and Water + Ethanol from (292.8 to 333.8) K, *2*(2), 3934–3936.
655 Romero, C. M., & Albis, A. (2010). Influence of polyols and glucose on the surface
656 tension of bovine α-lactalbumin in aqueous solution. *Journal of Solution*
657 *Chemistry*, *39*(12), 1865–1876. https://doi.org/10.1007/s10953-010-9554-5
658 Srinivas, K., King, J. W., Howard, L. R., & Monrad, J. K. (2010). Solubility and
659 solution thermodynamic properties of quercetin and quercetin dihydrate in
660 subcritical water. *Journal of Food Engineering*, *100*(2), 208–218.
661 https://doi.org/10.1016/j.jfoodeng.2010.04.001
662 Szymczyk, K., & Taraba, A. (2018). Thermodynamic study of quercetin and rutin
663 mixtures with alcohols. *Chemical Physics*, *505*, 6–11.
664 https://doi.org/10.1016/j.chemphys.2018.03.001
665 Tang, N., Zhong, J., & Yan, W. (2016). Solubilities of three flavonoids in different
666 natural deep eutectic solvents at T = (288.15 to 328.15) K. *Journal of Chemical*
667 *and Engineering Data*, *61*(12), 4203–4208.
668 https://doi.org/10.1021/acs.jced.6b00552
669 Tomé, L. I. N., Baião, V., da Silva, W., & Brett, C. M. A. (2018). Deep eutectic
670 solvents for the production and application of new materials. *Applied Materials*
671 *Today*, *10*, 30–50. https://doi.org/10.1016/j.apmt.2017.11.005
672 Wang, W., Sun, C., Mao, L., Ma, P., Liu, F., Yang, J., & Gao, Y. (2016). The biological
673 activities, chemical stability, metabolism and delivery systems of quercetin: A

review. *Trends in Food Science and Technology*, *56*, 21–38. https://doi.org/10.1016/j.tifs.2016.07.004

Zainal-Abidin, M. H., Hayyan, M., Hayyan, A., & Jayakumar, N. S. (2017). New horizons in the extraction of bioactive compounds using deep eutectic solvents: A review. *Analytica Chimica Acta*, *979*, 1–23. https://doi.org/10.1016/j.aca.2017.05.012

Żarska, M., Dzida, M., & Apelblat, A. (2017). Surface tensions and densities of concentrated aqueous solutions of citric acid. *Journal of Molecular Liquids*, *228*, 91–95. https://doi.org/10.1016/j.molliq.2016.07.019

Zhang, H., Wang, M., Chen, L., Liu, Y., Liu, H., Huo, H., … Qi, A. (2017). Structure-solubility relationships and thermodynamic aspects of solubility of some flavonoids in the solvents modeling biological media. *Journal of Molecular Liquids*, *225*, 439–445. https://doi.org/10.1016/j.molliq.2016.11.036

Zhao, B., Xu, P., Yang, F., Wu, H., Zong, M., & Lou, W. (2015). Biocompatible Deep Eutectic Solvents Based on Choline Chloride: Characterization and Application to the Extraction of Rutin from Sophora japonica. https://doi.org/10.1021/acssuschemeng.5b00619

Zhekenov, T., Toksanbayev, N., Kazakbayeva, Z., Shah, D., & Mjalli, F. S. (2017). Formation of type III Deep Eutectic Solvents and effect of water on their intermolecular interactions. *Fluid Phase Equilibria*, *441*, 43–48. https://doi.org/10.1016/j.fluid.2017.01.022